Spin dynamics and magnetic-field-induced polarization of excitons in ultrathin GaAs/AlAs quantum wells with indirect band gap and type-II band alignment

T. S. Shamirzaev[1,4], J. Rautert[2], D. R. Yakovlev[2,5], J. Debus[2],
A. Yu. Gornov[3], M. M. Glazov[5], E. L. Ivchenko[5], and M. Bayer[2,5]

[1] *Rzhanov Institute of Semiconductor Physics, Siberian Branch of the Russian Academy of Sciences, 630090 Novosibirsk, Russia*
[2] *Experimentelle Physik 2, Technische Universität Dortmund, 44227 Dortmund, Germany*
[3] *Institute for System Dynamics and Control Theory, Siberian Branch of the Russian Academy of Sciences, 664033 Irkutsk, Russia*
[4] *Ural Federal University, 620002 Yekaterinburg, Russia*
[5] *Ioffe Institute, Russian Academy of Sciences, 194021 St. Petersburg, Russia*

The exciton spin dynamics are investigated both experimentally and theoretically in two-monolayer-thick GaAs/AlAs quantum wells with an indirect band gap and a type-II band alignment. The magnetic-field-induced circular polarization of photoluminescence, P_c, is studied as function of the magnetic field strength and direction as well as sample temperature. The observed nonmonotonic behaviour of these functions is provided by the interplay of bright and dark exciton states contributing to the emission. To interpret the experiment, we have developed a kinetic master equation model which accounts for the dynamics of the spin states in this exciton quartet, radiative and nonradiative recombination processes, and redistribution of excitons between these states as result of spin relaxation. The model offers quantitative agreement with experiment and allows us to evaluate, for the studied structure, the heavy-hole g factor, $g_{hh} = +3.5$, and the spin relaxation times of electron, $\tau_{se} = 33$ μs, and hole, $\tau_{sh} = 3$ μs, bound in the exciton.

PACS numbers: 78.67.De,78.55.Cr, 85.75.-d

I. INTRODUCTION

Heterostructures with semiconductor quantum wells (QWs) have been interesting from several points of view including basic physics and optoelectronic devices [1, 2]. Among the different types of QWs, the longest exciton lifetimes up to milliseconds are obtained in indirect band-gap heterostructures with type-II band alignment [3]. Here the long lifetime is due to the separation of the oppositely charged carriers forming the excitons in real and momentum space. Since the electron spin relaxation times may reach milliseconds according to theoretical estimations [4, 5], type-II heterostructures, such as GaAs/AlAs QWs and superlattices, are highly interesting for studying long-lived exciton spin dynamics, which are not limited by exciton recombination. Recently, we demonstrated that an external magnetic field can control the intensity of the long-lived exciton recombination in type-II GaAs/AlAs QWs via redistribution of exciton population between bright and dark states [6]. However, the magnetic-field-induced polarization and the related spin dynamics of excitons in such QWs have been scarcely studied so far.

In this paper, we investigate the effects of a magnetic field on the exciton spin dynamics in ultrathin GaAs/AlAs QWs with indirect band gap and type-II band alignment. The circular polarization degree (P_c) of the QW exciton photoluminescence (PL) induced by a magnetic field shows an unusual behavior: (i) P_c has a strong spectral dependence across the emission band of the QW; it is small for the no-phonon (NP) line but its absolute value increases strongly for lines of phonon-assisted recombination. (ii) In tilted magnetic field $|P_c|$ demonstrates a monotonic increase with saturation in high fields, whereas in the Faraday or close-to-Faraday geometry P_c shows a non-monotonic behavior as function of the magnetic field B. Namely, the modulus of the polarization degree increases in low magnetic fields, reaches a maximum, and then decreases in strong fields. These experimental appearances are explained in the framework of a theoretical model based on the approach developed in our previous work [6].

The paper is organized as follows. In Sec. II the studied sample and used experimental techniques are described. In Sec. III we present the experimental data on the P_c of time-integrated and time-resolved PL recorded in external magnetic fields. The kinetic equation model, which accounts for the dynamics of the quartet of bright and dark exciton states in ultrathin GaAs/AlAs QWs, is presented in Sec. IV. The experimental data are analyzed in the frame of the model in Sec. V, which allows us to evaluate the carrier spin relaxation times and g factors. We show that the experimental data, being controlled by these parameters, can vary strongly, and we perform model calculations for several cases of interest for future experimental studies.

II. EXPERIMENTAL DETAILS

The ultrathin GaAs/AlAs QW structure studied here was grown by molecular-beam epitaxy on a semi-insulating (001)-oriented GaAs substrate in a Riber Compact system. The sample consists of the GaAs QW layer embedded between 50-nm-thick layers of AlAs grown on top of a 200-nm-thick GaAs buffer layer [7]. The sub-

strate temperature during the growth was 600°C. The GaAs QW layer was deposited with a nominal thickness of two monolayers. A 20-nm-thick GaAs cap layer protects the top AlAs layer against oxidation. Further growth details are given in Ref. [8]. The GaAs/AlAs QW has a type-II band alignment with the lowest conduction-band states at the X_x and X_y minima of the AlAs conduction band [3, 8, 9]. A schematic band diagram of the structure and the optical transition of the indirect exciton to the system ground state are presented in the inset of Fig. 1(b).

The sample was placed in a split-coil magnet cryostat and exposed to magnetic fields up to $B = 10$ T. The angle θ between the magnetic field direction and the QW growth axis (z axis) was varied between 0° (Faraday geometry) and 90° (Voigt geometry). For measurement of angular dependencies we fixed the magnetic field direction and rotated the sample. The emission was collected either in the direction along the field direction in Faraday geometry for $0° \leq \theta \leq 45°$ or perpendicular to the field direction in Voigt geometry for $45° < \theta \leq 90°$. The temperature was varied from $T = 1.8$ K up to 19 K. The photoluminescence was excited by the third harmonic of a Q-switched Nd:YVO_4 laser (3.49 eV) with a pulse duration of 5 ns. The pulse energy density was kept below 100 nJ/cm^2 and the pulse-repetition frequency was varied from 20 Hz up to 1 kHz [6].

The emitted light was dispersed by a 0.5-m monochromator. For time-integrated measurements the photoluminescence was detected by a liquid-nitrogen-cooled charge-coupled-device (CCD) camera. For the time-resolved measurements a GaAs photomultiplier combined with a time-correlated photon-counting module was used. In order to monitor the PL decay in a wide temporal range of up to 30 ms, the time resolution of the detection system (i.e. the binning range of the photon counting events) was varied between 3.2 ns and 6.4 μs.

The exciton spin dynamics were analyzed from the PL by measuring the circular polarization degree P_c induced by the external magnetic field. P_c was evaluated from the data by $P_c = [I_{\sigma^+} - I_{\sigma^-}]/[I_{\sigma^+} + I_{\sigma^-}]$, where I_{σ^+} and I_{σ^-} are the intensities of the σ^+ and σ^- polarized PL components, respectively. To determine the sign of P_c, we performed a control measurement on a diluted magnetic semiconductor structure with (Zn,Mn)Se/(Zn,Be)Se quantum wells for which $P_c > 0$ in Faraday geometry [10].

III. EXPERIMENTAL RESULTS

A time-integrated photoluminescence spectrum of the ultrathin GaAs/AlAs QW is shown in Fig. 1(a) by the black line. The spectrum comprises the contributions from several emission processes, as it contains the no-phonon (NP) line and several lines of phonon-assisted recombination involving optical and acoustic phonons from GaAs and AlAs. The replicas associated with the transverse acoustic (TA) phonons of AlAs (phonon energy of 12 meV) and the longitudinal optical (LO) phonons of GaAs (30 meV) and AlAs (48 meV), all at the X point of the Brillouin zone [11], can be distinguished. The lines are broadened due to the roughness of the QW interfaces [8]. An example of fitting of the PL spectrum with four contributing Gaussian curves, each with the same width of 19 meV, is shown in Fig. 1(a) by the red dotted line [6].

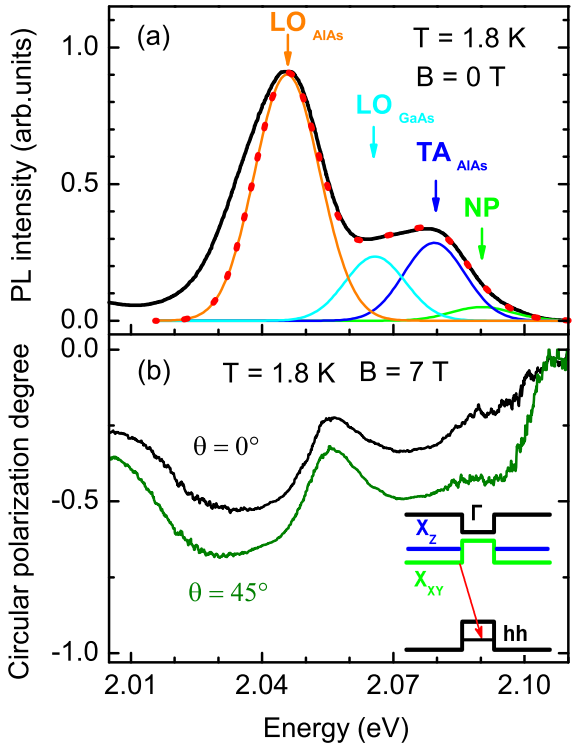

FIG. 1. (Color online) (a) Time-integrated PL spectrum of the ultrathin GaAs/AlAs QW (black line) fitted with four Gaussian lines corresponding to the exciton recombination with and without involvement of phonons. Green, blue, cyan, and orange solid lines are the no-phonon, TA_{AlAs}, LO_{GaAs} and LO_{AlAs} phonon lines, respectively. The red dotted line is the fitted spectrum composed of the four lines. (b) Spectral dependence of the PL circular polarization degree induced by a longitudinal ($\theta = 0°$) and a tilted ($\theta = 45°$) magnetic field B = 7 T. The inset shows the schematic band alignment of the structure with the QW in the middle. The red arrow marks the optical transition of the indirect exciton to the system ground state.

Application of a magnetic field results in polarization of the emission, as shown in Fig. 1(b) for $B = 7$ T in the Faraday geometry. One can see that P_c is negative (i.e., it isdominated by the σ^- polarized PL component) and has a strong spectral dependence. The absolute value of P_c equals to 0.17 for the NP line and increases up to 0.33 and 0.53 for the TA_{AlAs} and LO_{AlAs} phonon-assisted lines, respectively.

Next we take a closer look at the longitudinal magnetic field effect on the no-phonon and phonon-assisted

lines. Since the intensities of the σ^+ and σ^- polarized PL components are proportional to the populations of the exciton Zeeman sublevels, P_c reflects these populations. The $P_c(B)$ dependencies of these lines measured in longitudinal magnetic field are shown in Fig. 2. For all lines the polarization degree increases in low magnetic fields, reaches a maximum, and then decreases in strong fields. The maximal value of the polarization degree, $|P_{c,max}|$, is achieved at magnetic fields of B_{max} = 3.7 T, 4.6 T, and 5 T for the NP, TA_{AlAs} and LO_{AlAs} lines, respectively. While the difference of B_{max} for the TA and LO phonon replicas is negligible, the NP line strongly deviates from the phonon replicas. The origin of this line is not well established [6]: In particular, it may be related with trions, i.e., negatively charged excitons. In that case, the selection rules are strongly different from those for neutral excitons. Therefore, we exclude this line from the analysis. Note that all replicas show similar changes in intensity, dynamics [6] and polarization with varying temperature, magnetic field strength and sample orientation. Therefore, we will focus on the properties of the phonon-assisted LO_{AlAs} line.

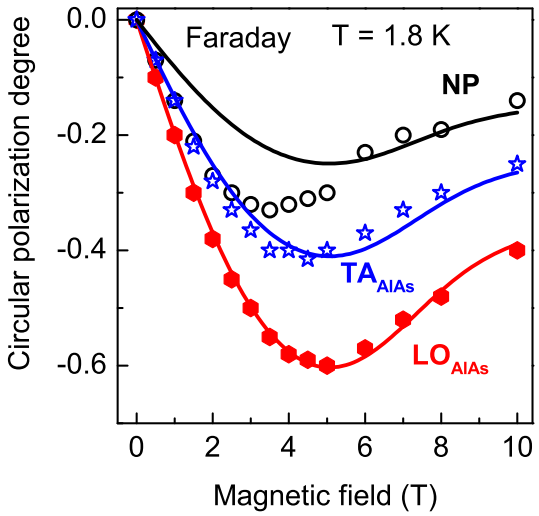

FIG. 2. (Color online) Circular polarization degree induced by a longitudinal magnetic field as function of field strength for the NP (open circles), TA_{AlAs} (open stars) and LO_{AlAs} (full hexagons) lines, respectively. Lines show results of modeling with parameters given in Sec. V A.

The $P_c(B)$ dependencies for the LO_{AlAs} line at various temperatures are shown in Fig. 3. With increasing temperature the slope of the polarization rise monotonically decreases and the $P_{c,max}$ value is shifted towards stronger magnetic fields. For a fixed longitudinal magnetic field of 9 T, $P_c(T)$ demonstrates an unexpected nonmonotonic dependence as shown in Fig. 4. The absolute value of the polarization degree increases from 0.45 up to 0.59 with increasing temperature from 2 up to 4.2 K. Then, it steadily decreases down to 0.15 with further temperature increase to 19 K.

The $P_c(B)$ of the phonon-assisted lines depends

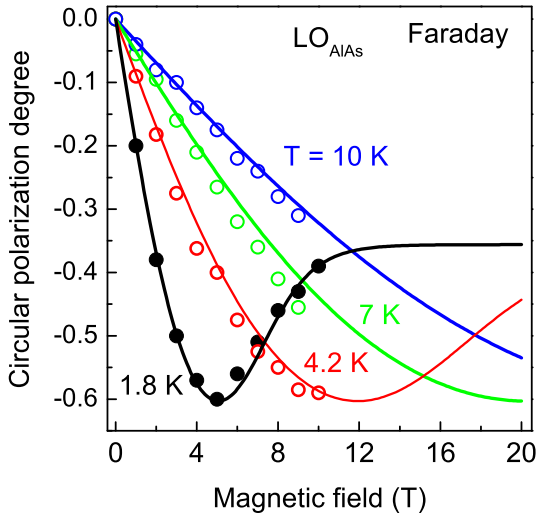

FIG. 3. (Color online) Magnetic-field-induced circular polarization degree of LO_{AlAs} phonon-assisted transition measured at temperatures of 1.8, 4.2, 7 and 10 K (symbols). Lines show results of modeling with parameters given in Sec. V A.

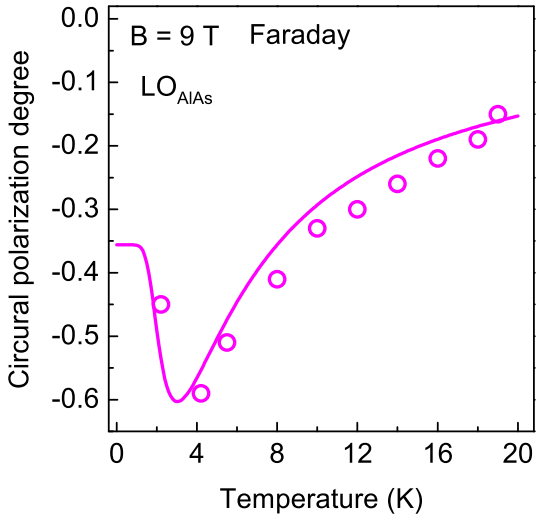

FIG. 4. (Color online) Magnetic-field-induced circular polarization degree of the LO_{AlAs} phonon-assisted transition at $B = 9$ T as function of temperature. Circles give experimental data and line is the modeling result with the parameters given in Sec. V A.

strongly on the experimental geometry as shown in Fig. 5. It behaves nonmonotonically in the Faraday geometry, while a finite angle θ between the magnetic field direction and the QW growth axis unexpectedly suppresses the decrease of $|P_c|$ in high magnetic fields. $|P_c(B)|$ for a field tilt by 45° from the Faraday geometry increases monotonically and saturates at 0.72 for 10 T. However, as one can see in Fig. 1(b), the spectral dependence of the polarization degree in the tilted geometry is pronounced and similar to that in the Faraday geometry.

In order to analyze in more detail the angular de-

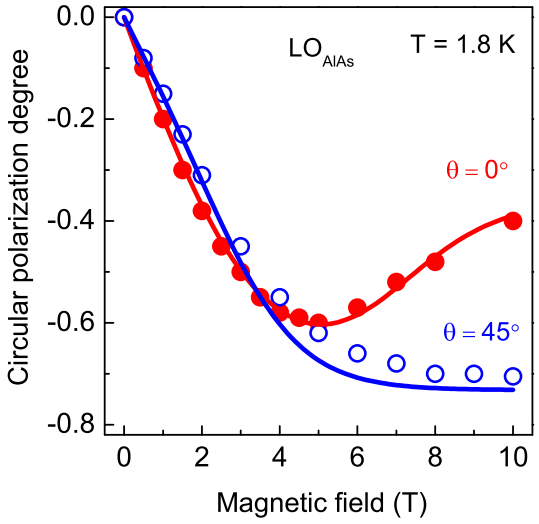

FIG. 5. (Color online) Magnetic-field-induced circular polarization degree of the LO_{AlAs} phonon-assisted transition, in longitudinal (closed red circles) and tilted by 45° (open blue circles) field configuration as function of the field strength. Lines are the modeling results with the parameters given in Sec. V A.

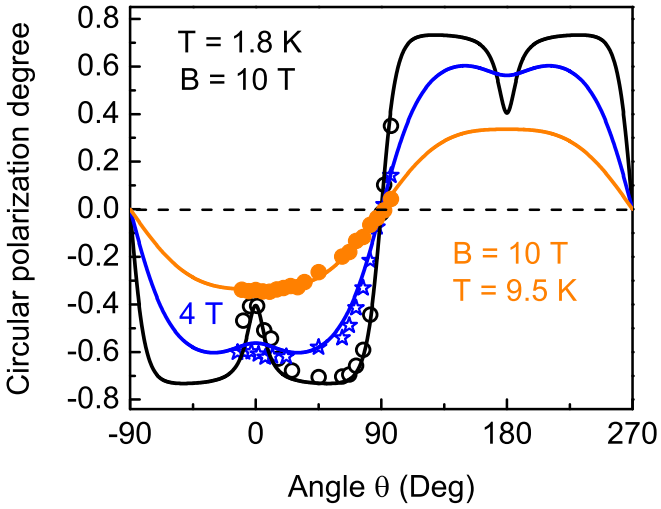

FIG. 6. (Color online) Angle dependencies of $P_c(\theta)$ measured at temperature $T = 1.8$ K for $B = 4$ T (open blue stars) and 10 T (open black circles), and at $T = 9.5$ K for $B = 10$ T (full orange circles). Lines show results of the modeling with the parameters given in text.

pendence of the polarization degree, we measured it at $T = 1.8$ K for $B = 4$ and 10 T, and at $T = 9.5$ K for $B = 10$ T. These results are shown in Fig. 6. For low magnetic fields, where $|P_c|$ is smaller than its maximal value $|P_{c,max}|$ in longitudinal magnetic field, the polarization degree changes weakly up to about $\theta = 45°$, and goes to zero for θ increased further to 90° (Voigt geometry). In higher magnetic fields P_c increases for $0° < \theta < 30°$, changes insignificantly in the range of $30° < \theta < 60°$, and goes to 0 for θ enlarged towards 90°. For any magnetic field an increase of θ beyond 90° results in a change of the polarization sign; the PL is dominated then by the σ^+ polarized component. With increasing temperature up to 9.5 K at $B = 10$ T, the polarization $|P_c(\theta)|$ monotonically decreases when θ is varied from 0 to 90°.

The PL dynamics for different magnetic field strengths and geometries for the two circular polarized components, i.e. $I_{\sigma^+}(t)$ and $I_{\sigma^-}(t)$, and the dynamics of the circular polarization degree $P_c(t) = [I_{\sigma^+}(t) - I_{\sigma^-}(t)]/[I_{\sigma^+}(t) + I_{\sigma^-}(t)]$ are shown in Fig. 7. The circular polarization is very small for short delay times, then it increases within a characteristic time of $\tau_s = 3$ μs, which is much shorter than the exciton PL decay time [6]. It is interesting that the change in magnetic field strength and geometry results in a modification of the maximal value of the polarization degree only, while τ_s remains basicly constant in the whole scanned B and θ range.

In conclusion of this section, we summarize the most important experimental findings:

(i) The magnetic-field-induced circular polarization degree P_c has a complicated spectral dependence.

(ii) In the Faraday (and close-to-Faraday) geometry the absolute value of $|P_c|$ increases in low magnetic fields and decreases in strong fields. However, in tilted magnetic field, $|P_c(B)|$ demonstrates a monotonic increase with saturation in strong fields.

(iii) In the Voigt geometry the circular polarization degree $P_c = 0$. Varying θ from 90° by a few degrees leads to a rapid increase in P_c.

(iv) The temperature dependence of P_c is also non-monotonic. In high magnetic fields the absolute value of the polarization degree increases with increasing temperature from 2 up to 4.2 K, and then it monotonically decreases with further temperature increase.

IV. THEORY

In this section we present a kinetic theory of the photoluminescence polarization in monolayer-thin GaAs/AlAs quantum wells. In Sec. IV A we introduce the kinetic equations for the occupancies of the quadruplet of exciton spin sublevels. In Sec. IV B we present the analytical solution of these kinetic equations for arbitrary strength and direction of the magnetic field. We analyze various limiting cases of the Faraday and Voigt geometries in Secs. IV C and IV D, respectively, and address the selection rules in Sec. IV E.

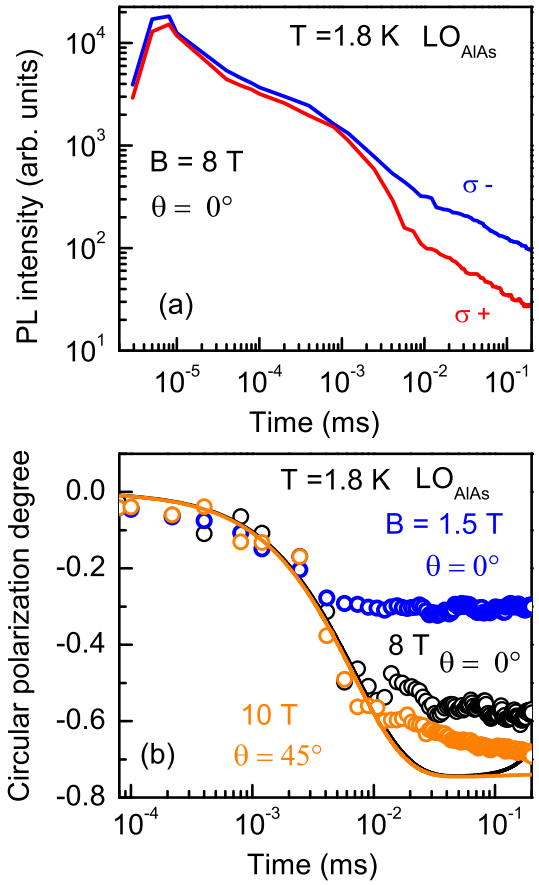

FIG. 7. (Color online) (a) Recombination dynamics of the σ^+ and σ^- polarized PL components of the LO_{AlAs} emission line, measured at $T = 1.8$ K in the Faraday geometry for $B = 8$ T. (b) Dynamics of the circular polarization degree of the LO_{AlAs} emission line measured at $T = 1.8$ K for different magnetic field strengths and geometries: $B = 1.5$ T (blue symbols) and 8 T (black symbols) in the Faraday geometry, and $B = 10$ T (orange symbols) tilted by 45°. Solid lines show the model results for $B = 8$ T (black line) in the Faraday geometry and $B = 10$ T (orange line) for $\theta = 45°$ with the parameters given in text. The calculations of $P_c(t)$ dynamics are made via Eq. (11) using the solution of Eqs. (12) for pulsed excitation. The parameters are given in Sec. V A.

A. Kinetic equations for the occupation probabilities of exciton spin sublevels

We consider the quadruplet of exciton states formed by a conduction-band electron and a heavy hole in the valence band. Following the model of Ref. [6] we neglect the exchange interaction between the electron and the hole and assume that the electron Zeeman effect in $X_{x,y}$-valleys is isotropic, i.e., the in- and out-of-plane components of the g factor are equal. By contrast, we completely disregard the in-plane magnetic field effect on the heavy-hole spin. As a result, the eigenstates of the hole are still characterized by the z-component of the angular momentum, $j_z = \pm 3/2$, and denoted as $|\pm 3/2\rangle_z$. The electron eigenstates $|s\rangle_{\boldsymbol{B}}$ are characterized by the spin component $s = \pm 1/2$ onto the magnetic field direction and form the superpositions of the basic functions $|\pm 1/2\rangle_z$:

$$|+1/2\rangle_{\boldsymbol{B}} = C|1/2\rangle_z + D|-1/2\rangle_z\,, \qquad (1)$$
$$|-1/2\rangle_{\boldsymbol{B}} = -D|1/2\rangle_z + C|-1/2\rangle_z\,.$$

Here, the subscripts z and $\boldsymbol{B}$ are introduced in order to highlight the difference between the basic spinors and the eigenfunctions of the Zeeman Hamiltonian, the coefficients C and D (normalized to unity) depend on the magnetic field orientation. If the magnetic field is tilted by the angle θ with respect to the sample normal in the (xz) plane the coefficients in Eq. (1) take the simple form:

$$C = \cos(\theta/2), \quad D = \sin(\theta/2). \qquad (2)$$

Hence, the exciton spin state is represented as a product of the electron and the heavy-hole eigenstates

$$|sj_z\rangle = |s\rangle_{\boldsymbol{B}}|j_z\rangle_z,$$

and labeled by the pair of electron and hole spin components, s and j_z. Within the model presented in Ref. [6], which accounts for spin flips of the electron and hole as well as the radiative and nonradiative recombination of the exciton, the occupancies, f_{sj_z}, of the exciton states obey the following set of kinetic equations:

$$\frac{df_{sj_z}}{dt} + \left(W_{\bar{s},s} + W_{\bar{j}_z,j_z}\right) f_{sj_z} - W_{s,\bar{s}} f_{\bar{s}j_z} - W_{j_z,\bar{j}_z} f_{s\bar{j}_z} + \mathcal{R} f_{sj_z} = G_{sj_z}\,. \qquad (3)$$

Here $\bar{s} = -s$, $\bar{j}_z = -j_z$, $W_{s,s'}$ (W_{j_z,j'_z}) are the electron (heavy-hole) spin-flip rates for the transitions $s' \to s$ $(j'_z \to j_z)$, the operator $\mathcal{R}$ describes the radiative and nonradiative recombination of excitons, and G_{sj_z} is the exciton generation rate in the state $|sj_z\rangle$. In accordance with Ref. [6] we present the energies of the exciton sublevels E_{sj_z} in the form

$$E_{sj_z} = g_e s \mu_B B + \frac{g_{hh}}{3} j_z \mu_B B_z, \qquad (4)$$

where μ_B is the Bohr magneton, g_e and g_{hh} are the electron and heavy-hole Landé factors, B is the total magnetic field, B_z is its z component. In the experiment the Zeeman splittings can be comparable with the thermal energy, $k_B T$, where T is the sample temperature and k_B is the Boltzmann constant. Hence, the rates of the transitions from the lower to higher and from the higher to lower Zeeman sublevels are different and can be interrelated as

$$W_{1/2,-1/2} = W_{-1/2,1/2} \exp\left(-\frac{g_e \mu_B B}{k_B T}\right), \qquad (5)$$
$$W_{3/2,-3/2} = W_{-3/2,3/2} \exp\left(-\frac{g_{hh} \mu_B B_z}{k_B T}\right).$$

Both electron and hole Landé factors are positive in the studied sample, moreover, $g_{hh} > g_e$ [6]. Then, without

loss of generality, we choose the positive direction of the z axis to have $B_z > 0$ and represent the transition rates in the form

$$W_{-1/2,1/2} \equiv w_e, \quad W_{-3/2,3/2} \equiv w_h, \qquad (6)$$
$$W_{1/2,-1/2} = \alpha w_e, \quad W_{3/2,-3/2} = \beta w_h,$$

where the Boltzmann factors in Eqs. (5) are denoted as

$$\alpha = \exp\left(-\frac{g_e \mu_B B}{k_B T}\right), \quad \beta = \exp\left(-\frac{g_{hh} \mu_B B_z}{k_B T}\right), \quad (7)$$

and $\alpha, \beta \leqslant 1$. The rates w_e, w_h represent the spin-flip transitions downwards in energy, their dependence on magnetic field is relatively weak and described by power laws [5, 12, 13] and is disregarded hereafter. In the following we simplify the notation for the occupation probability and replace f_{sj_z} ($s = \pm 1/2, j_z = \pm 3/2$) just by f_{ij} with $i = \pm$ and $j = \pm$ indicating the signs of s and j_z, respectively.

Let us now establish the selection rules governing the phonon-assisted exciton recombination in ultrathin GaAs/AlAs quantum wells, characterized by an indirect band gap and a type-II band alignment. It is commonly accepted that the recombination of the exciton in such system is related with (i) the spin-conserving virtual transition of the electron from the X_x or X_y valley to the Γ-point accompanied by phonon emission and (ii) the recombination of the exciton at the Brillouin zone center [6, 14, 15]. At the Γ-point the strict selection rules involving the periodic Bloch amplitudes of the $|\Gamma_6, s_z\rangle$ conduction band electron state and the $|\Gamma_8, j_z\rangle$ valence band hole state characterized by their spin z-components s_z, j_z read

$$|\Gamma_6, 1/2; \Gamma_8, -3/2\rangle \to \sigma_- \,, \; |\Gamma_6, -1/2; \Gamma_8, 3/2\rangle \to \sigma_+, \quad (8)$$
$$|\Gamma_6, 1/2; \Gamma_8, 1/2\rangle \to \sigma_+ \,, \; |\Gamma_6, -1/2; \Gamma_8, -1/2\rangle \to \sigma_- \,,$$
$$|\Gamma_6, 1/2; \Gamma_8, 3/2\rangle, \; |\Gamma_6, -1/2; \Gamma_8, -3/2\rangle \to \text{forbidden} \,,$$
$$|\Gamma_6, 1/2; \Gamma_8, -1/2\rangle, |\Gamma_6, -1/2; \Gamma_8, 1/2\rangle \to z\text{-polarized} \,.$$

Neglecting the mixing of the hole states we obtain that only the exciton states with $s_z = -1/2, j_z = 3/2$ and $s_z = 1/2, j_z = -3/2$ are active (bright) in σ^+ and σ^- polarization [6, 16], respectively. These selection rules result in the following form of the recombination operator $\mathcal{R}$:

$$\mathcal{R} f_{-+/+-} = \left(\frac{1}{\tau_{nr}} + \frac{C^2}{\tau_r}\right) f_{-+/+-}, \qquad (9)$$
$$\mathcal{R} f_{++/--} = \left(\frac{1}{\tau_{nr}} + \frac{D^2}{\tau_r}\right) f_{++/--},$$

where the subscript $-+/+-$ means $-+$ *or* $+-$, τ_{nr} and τ_r are the nonradiative and radiative recombination times of the excitons, and the coefficients C, D are defined by Eq. (2). The heavy-hole exciton emits light which propagates along the quantum well normal. Correspondingly, the intensities of the exciton emission in σ^+ and σ^- polarization are given by

$$I_{+/-} \propto \frac{C^2}{\tau_r} f_{-+/+-} + \frac{D^2}{\tau_r} f_{++/--} \,. \qquad (10)$$

Therefore, one obtains for the degree of circular polarization of the emission

$$P_c = \frac{C^2(f_{-+} - f_{+-}) + D^2(f_{++} - f_{--})}{C^2(f_{-+} + f_{+-}) + D^2(f_{++} + f_{--})}. \qquad (11)$$

Deviations from these strict selection rules are addressed in Sec. IV E.

For arbitrary orientation of the external magnetic field in the interval $0 \leq \theta \leq \pi/2$, we get from Eqs. (3), (6) and (9):

$$\frac{df_{--}}{dt} + \left(D^2 w + w'\right) f_{--} + w_e(\alpha f_{--} - f_{+-}) + w_h(\beta f_{--} - f_{-+}) = G_{--} \,, \qquad (12)$$
$$\frac{df_{++}}{dt} + \left(C^2 w + w'\right) f_{++} + w_e(f_{++} - \alpha f_{-+}) + w_h(f_{++} - \beta f_{+-}) = G_{++} \,,$$
$$\frac{df_{+-}}{dt} + \left(w' + C^2 w\right) f_{+-} + w_e(f_{+-} - \alpha f_{--}) + w_h(\beta f_{+-} - f_{++}) = G_{+-} \,,$$
$$\frac{df_{-+}}{dt} + \left(w' + D^2 w\right) f_{-+} + w_e(\alpha f_{-+} - f_{++}) + w_h(f_{-+} - \beta f_{--}) = G_{-+} \,,$$

where $w = 1/\tau_r$ and $w' = 1/\tau_{nr}$. Note that for $\theta = 0$, i.e., for the Faraday geometry, a similar set of kinetic equations describing bright and dark exciton spin dynamics was presented in Ref. [17]. This model is sufficient to describe the recombination dynamics of excitons observed in Ref. [6] and, as shown below, readily accounts for most

of the present experimental observations.

B. Analytical solution of the set (12) in the steady-state regime

Under steady-state photoexcitation the time derivatives in Eqs. (12) vanish, $df_{sj_z}/dt = 0$. Here and in what follows we focus on the important limit of equal generation rates in all exciton states, $G_{ij} \equiv G$, which is relevant for the experimental situation of interest. Making use of the firs t two equations of the set (12) one can express the occupancies of the (in the Faraday geometry) dark states, f_{++} and f_{--} through the occupancies of the bright states f_{-+}, f_{+-} as follows

$$\begin{aligned} f_{--} &= \frac{G + w_e f_{+-} + w_h f_{-+}}{\tilde{w}' + \alpha w_e + \beta w_h}\,, \\ f_{++} &= \frac{G + \alpha w_e f_{-+} + \beta w_h f_{+-}}{\tilde{w}' + w_e + w_h}\,, \end{aligned} \tag{13}$$

where $\tilde{w}' = w' + D^2 w$. Substituting these expressions into the two last equations (12), we arrive at the following equations for the bright-state populations

$$\begin{aligned} &(w_{+-} + \beta W)\, f_{+-} - \alpha W f_{-+} = \tilde{G}_{+-}\,, \\ &-\beta W f_{+-} + (w_{-+} + \alpha W)\, f_{-+} = \tilde{G}_{-+}\,. \end{aligned} \tag{14}$$

Here the effective generation rates

$$\begin{aligned} \tilde{G}_{+-} &= G\left(1 + \frac{\alpha w_e}{\tilde{w}' + \alpha w_e + \beta w_h} + \frac{w_h}{\tilde{w}' + w_e + w_h}\right), \\ \tilde{G}_{-+} &= G\left(1 + \frac{w_e}{\tilde{w}' + w_e + w_h} + \frac{\beta w_h}{\tilde{w}' + \alpha w_e + \beta w_h}\right),. \end{aligned}$$

The rates w_{-+}, w_{+-}, W are defined by

$$\begin{aligned} w_{-+} &= \tilde{w} + \tilde{w}'\left(1 + \frac{\alpha w_e}{\tilde{w}' + w_e + w_h} + \frac{w_h}{\tilde{w}' + \alpha w_e + \beta w_h}\right), \\ w_{+-} &= \tilde{w} + w'\left(1 + \frac{w_e}{\tilde{w}' + \alpha w_e + \beta w_h} + \frac{\beta w_h}{\tilde{w}' + w_e + w_h}\right), \\ W &= w_e w_h\left(\frac{1}{\tilde{w}' + \alpha w_e + \beta w_h} + \frac{1}{\tilde{w}' + w_e + w_h}\right), \end{aligned}$$

and $\tilde{w} = (C^2 - D^2)w + w'$. As a result we obtain for the bright state populations

$$\begin{aligned} f_{-+} &= \frac{(w_{+-} + \beta W)\,\tilde{G}_{-+} + \beta W \tilde{G}_{+-}}{w_{-+}w_{+-} + (w_{+-}\alpha + w_{+-}\beta)\,W}\,, \\ f_{+-} &= \frac{(w_{-+} + \alpha W)\,\tilde{G}_{+-} + \alpha W \tilde{G}_{-+}}{w_{-+}w_{+-} + (w_{+-}\alpha + w_{+-}\beta)\,W}\,. \end{aligned} \tag{15}$$

The populations of the dark states $--/++$, namely, f_{--} and f_{++}, are expressed via the bright ones f_{+-} and f_{-+} by virtue of Eq. (13).

C. Faraday geometry, important limiting case

In the longitudinal magnetic field $\mathbf{B} \parallel z$ ($C^2 = 1, D^2 = 0$), Eq. (11) for the circular polarization degree reduces to

$$P_c = \frac{f_{-+} - f_{+-}}{f_{-+} + f_{+-}}. \tag{16}$$

In this subsection we consider the important limiting case of a sufficiently strong field, so that

$$\alpha, \beta \ll 1. \tag{17}$$

Further, we consider a weak nonradiative decay and an efficient spin relaxation from the higher to the lower Zeeman sublevels

$$w' \ll w \ll w_e, w_h, \tag{18}$$

while the relations between $w', \alpha w_e$ and βw_h remain unrestricted. Then the following simplifications are possible

$$\begin{aligned} \tilde{G}_{-+} &\approx G\left(1 + \frac{\alpha w_e}{w' + \alpha w_e + \beta w_h} + \frac{w_h}{w_e + w_h}\right), \\ \tilde{G}_{+-} &\approx G\left(1 + \frac{w_e}{w_e + w_h} + \frac{\beta w_h}{w' + \alpha w_e + \beta w_h}\right), \\ w_{-+} &\approx \frac{w' w_e}{w' + \alpha w_e + \beta w_h}\,, \\ w_{+-} &\approx \frac{w' w_h}{w' + \alpha w_e + \beta w_h}\,, \\ W &\approx \frac{w_e w_h}{w' + \alpha w_e + \beta w_h}\,, \end{aligned} \tag{19}$$

with the result

$$\begin{aligned} f_{-+} &= \frac{G}{w_h}\left(1 + \frac{w_e}{w_e + w_h} + 4\beta\frac{w_h}{w'}\right), \\ f_{+-} &= \frac{G}{w_e}\left(1 + \frac{w_h}{w_e + w_h} + 4\alpha\frac{w_e}{w'}\right). \end{aligned} \tag{20}$$

Equations (20) can be obtained by using simple considerations, namely by (i) analyzing the case of very strong magnetic fields where only transitions with phonon emission are possible and (ii) taking into account the phonon absorption in first-order perturbation theory. First, we completely neglect transitions accompanied with phonon absorption, i.e., we set $\alpha, \beta = 0$ and obtain from Eqs. (12)

$$f_{++} = \frac{G}{w_e + w_h}, \quad f_{+-} = \frac{G}{w_e}\left(1 + \frac{w_h}{w_e + w_h}\right) \tag{21a}$$

$$f_{-+} = \frac{G}{w_h}\left(1 + \frac{w_e}{w_e + w_h}\right), \quad f_{--} = 4G/w'. \tag{21b}$$

This result is valid in very strong magnetic fields, shown in Fig. 8 as region III, where $\alpha w_e \tau_{nr}, \beta w_h \tau_{nr} \ll 1$. Note that since the polarization is controlled by the transitions from the states $|{-+}\rangle$ and $|{+-}\rangle$, it shows a dynamic behavior. Indeed, the sign of polarization is determined

by the state which is emptied slower. If $w_h < w_e$ so that the electron spin flip is fastest, the population of the state $|+-\rangle$ decays faster towards the ground sublevel $|--\rangle$ and the value of P_c is positive. By contrast, for $w_h > w_e$, the state $|-+\rangle$ decays faster and P_c becomes negative. This is in agreement with Eq. (16) which can be recast as

$$P_c = \frac{1-\zeta^2}{1+\zeta+\zeta^2}, \quad \zeta = \frac{w_h}{w_e}. \tag{22}$$

For moderate magnetic fields according to Eq. (17), shown in Fig. 8 as region II, it is sufficient to take into account additionally the transitions from the ground sublevel $|--\rangle$ to the $|-+\rangle$, $|+-\rangle$ sublevels only. This results in the modification of the bright-state occupations from (21) to (20) and of the polarization from Eq. (16) to

$$P_c = \frac{w_e^2 - w_h^2 + 2\tau_{nr}(\beta-\alpha)(w_e+w_h)w_e w_h}{w_e^2 + w_h^2 + w_e w_h[1 + 2\tau_{nr}(\beta+\alpha)(w_e+w_h)]}, \tag{23}$$

while f_{++}, f_{--} remain unchanged.

Finally, in the weak-field limit (region I in Fig. 8) $\alpha w_e \tau_{nr}, \beta w_h \tau_{nr} \gg 1$ the spin relaxation is fast as compared with the recombination processes, so that the states $|-+\rangle$, $|+-\rangle$ become thermally populated and one obtains

$$P_c = \frac{1-\chi}{1+\chi}, \quad \chi = \exp\left(-\frac{(g_e - g_{hh})\mu_B B}{k_B T}\right). \tag{24}$$

In fact, for the parameters of the experimentally studied structure (see Sec. V A for the specific values) Eq. (24) holds for magnetic fields from $B_z = 0$ to $B_z \approx 3$ T at the lowest accessible temperatures.

D. The Voigt geometry

It is also instructive to address the Voigt geometry, $\boldsymbol{B} \parallel x$, in which case the coefficients $C = D = 1/\sqrt{2}$. The electron spin states then read

$$|\pm 1/2\rangle_{\boldsymbol{B}} = \frac{1}{\sqrt{2}}(|1/2\rangle_z \pm |-1/2\rangle_z)\,.$$

Here the radiative decay rates of all four states are the same. Moreover, the exciton states sj_z form two degenerate pairs $(++, --)$ and $(+-, -+)$ because the effect of the in-plane field is disregarded. As a result, according to Eqs. (13) and (15) the populations f_{ij} are given by

$$\begin{aligned} f_{++} = f_{--} &= \frac{G}{\frac{w}{2}+w'}\,\frac{\frac{w}{2}+w'+2w_e}{\frac{w}{2}+w'+(1+\alpha)w_e}\,, \\ f_{+-} = f_{-+} &= \frac{G}{\frac{w}{2}+w'}\,\frac{\frac{w}{2}+w'+2\alpha w_e}{\frac{w}{2}+w'+(1+\alpha)w_e}. \end{aligned} \tag{25}$$

In the Voigt geometry there is no circular polarization P_c of the emission. The emission intensity is weakly affected by the magnetic field.

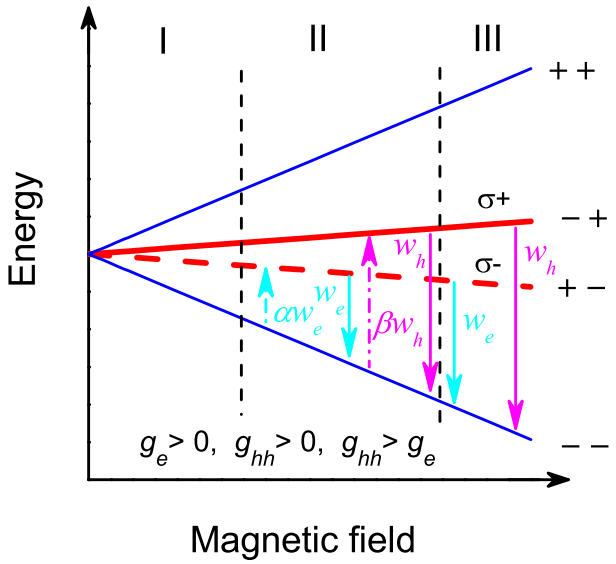

FIG. 8. (Color online) Schematic illustration of the indirect-exciton spin levels in Faraday geometry, $\boldsymbol{B} \parallel z$. The blue lines show optically dark (spin-forbidden) states, the red lines show spin allowed bright states in σ^+ (solid line) and σ^- (dash line) polarization. Arrows demonstrate electron (hole) spin-flip processes increasing and decreasing the energy, respectively, with rates αw_e (βw_h) and w_e (w_h). The regions I, II, and III indicate the cases of weak, moderate, and high magnetic fields, respectively. For definiteness the case of positive g_e, g_{hh} with $g_{hh} > g_e$, which provides an interpretation of the main experimental findings, is shown.

E. Possible deviation of selection rules

The above model already accounts for the majority of experimental observations in the present work and in Ref. [6]. However, in order to describe particular features of the observed dynamics of the exciton luminescence polarization, we need to allow for minor deviations of the selection rules from those in Eq. (8). As we demonstrate below these deviations are important mostly in the Faraday geometry. Therefore we focus on this specific geometry, $\boldsymbol{B} \parallel z$, and specify the states by the exciton angular momentum component $m_z = s_z + j_z$. We assume the structure under study to have C_{2v} point symmetry. In this case the bright exciton states, ± 1, are mixed with each other, while the dark states, ± 2, can be mixed with the excited (light-hole exciton) states with $m_z = 0$. As a result, the selection rules deviate from those described above.

In the simplest model of symmetry reduction from the D_{2d} point group that is relevant for [001]-grown quantum wells with symmetric heteropotential and equivalent interfaces, let us take into account mixing of the heavy-hole, $|\Gamma_8, \pm 3/2\rangle$, and the light-hole, $|\Gamma_8, \mp 1/2\rangle$, states. Microscopically, the mixing is related to the anisotropy of the chemical bonds at the interfaces, strain and/or

anisotropic localization [16] and described by

$$\left|\pm\frac{3}{2}\right\rangle = \mathcal{N}\left(\varphi_h(z)\left|\Gamma_8,\pm\frac{3}{2}\right\rangle + \eta\varphi_l(z)\left|\Gamma_8,\mp\frac{1}{2}\right\rangle\right). \tag{26}$$

Here $\varphi_h(z)$, $\varphi_l(z)$ are the envelope functions of the heavy- and light-hole states, η is the admixture coefficient, and $\mathcal{N} = 1/\sqrt{1+|\eta|^2}$ is the normalization constant. The phase of the admixture coefficient is determined by the choice of axes in the quantum well plane. The admixture of light hole states results in a modification of the selection rules: Each of the "bright" states with $|m_z| = 1$ is active, both in σ^+ and σ^- polarization, with a strength given by the ratio of the squared moduli of the matrix elements

$$\frac{|M_{\sigma^-}(-1/2,+3/2)|}{|M_{\sigma^+}(-1/2,+3/2)|} = \frac{|M_{\sigma^+}(+1/2,-3/2)|}{|M_{\sigma^-}(+1/2,-3/2)|} = \frac{|\eta|}{\sqrt{3}}. \tag{27}$$

The dark states should become weakly ($|M|^2 \propto |\eta|^2$) optically active in the z polarization (normal to the QW plane), this emission is, however, not detected in the experimental geometry. Hence, the heavy-light hole mixing results in a partial depolarization of the exciton emission.

Moreover, besides the mixing of heavy- and light hole described by Eq. (26), we allow for spin-flip processes in the phonon-assisted recombination which result in an activation of the dark states, $|m_z| = 2$, in the in-plane polarization. For better agreement with experiment we assume that the state with $m_z = -2$ is weakly active in the σ^+ polarization and, reciprocally, the state with $m_z = +2$ is weakly active in the σ^- polarization. As a result, in the Faraday geometry, we write the degree of exciton luminescence circular polarization as follows

$$P_c = \xi\frac{f_{+1} - f_{-1} + C_d(f_{-2} - f_{+2})}{f_{+1} + f_{-1} + C'_d(f_{-2} + f_{+2})}. \tag{28}$$

Here $\xi = (3-|\eta|^2)/(3+|\eta|^2)$ is the depolarization factor and the positive coefficients $C_d, C'_d \ll 1$ account for the emission of the dark states. Setting $\xi = 1$ and $C_d, C'_d = 0$ we return to the strict selection rules of Eq. (8). Generally, the parameters ξ and C_d, C'_d can depend on the phonon involved in the replica formation. For example, due to interface effects, the coupling of excitons to the short-wavelength phonons involved in the indirect photoemission can depend on the localization site (e.g., through the localization energy and, therefore, the localization length) and this dependence can be different for the TA and LO phonons. Then the emitting states participating in the TA- and LO-assisted photoluminescence processes can differ in the heavy-light hole mixing strength, the depolarization factor ξ and the dark-state activation factors C_d, C'_d. In the following for simplicity we set $C_d = C'_d$.

V. MODELING THE EXPERIMENTAL RESULTS

We consider here a Wannier–Mott exciton formed by an electron in the doubly-degenerate conduction band and a hole in the doubly-degenerate valence band. For (001)-grown heterostructures with zinc-blende lattice, two of the exciton quartet states are bright and the two other states are dark. The bright excitons can be directly excited by light and can emit light. The dark excitons are optically inactive, they recombine with a nonradiative decay rate, have a longer lifetime and can act as a reservoir of excitons. The electron-hole exchange interaction results in a splitting between the bright and dark doublets and, due to reduced symmetry of a particular nanosystem, in an additional splitting of each doublet. Moreover, the exciton fine structure can be controlled by an external magnetic field which produces a three-fold effect: (i) it modifies and increases the sublevel splitting, (ii) it mixes the bright and dark states (at tilted fields or in the Voigt geometry), and (iii) it induces level crossing or anticrossing.

The population of the split sublevels is arranged by the interplay between recombination processes and spin flips of either an electron or a hole between the sublevels. Thus, the exciton photoluminescence intensity and polarization are governed by the following set of parameters: the exchange constants, the values and signs of the electron and hole g factors (together with the strength and orientation of the magnetic field), the radiative (τ_r) and nonradiative (τ_{nr}) recombination times, the spin relaxation rates (w_e, w_h) describing the spin flip rates for downward transitions, i.e., from the upper to the lower Zeeman sublevel, and the temperature which determines the ratio of upward and downward transitions. The possibility of various relations between the above parameters for the quartet excitons offers a vast diversity.

One of the simplest cases is realized in colloidal CdTe nanocrystals where due to the strong confinement the bright-dark exchange splitting exceeds by far the Zeeman energy (in the studied range of magnetic fields) and the thermal energy k_BT. Hence, in this material system at liquid helium temperatures the thermally induced mixing between bright- and dark-exciton states can be neglected, and only thermalization between the Zeeman levels of the bright excitons has to be taken into account [17].

The quantum confinement of electrons and holes in InAs/(In,Al,Ga)As self-assembled quantum dots suppresses the most efficient spin relaxation mechanisms so that the spin flip processes in the exciton are much slower than the radiative recombination [18]. As for the exchange interaction energy, it is small compared with the electron and hole Zeeman energies even in a moderate magnetic field of $B = 0.5$ T.

In studies of pseudo-direct GaAs/AlAs superlattices where the Γ-X mixing is responsible for the nanosecond scale of the exciton radiative time, see e.g. [19, 20], the exchange and Zeeman splittings are small as compared

with the thermal energy at liquid-helium temperature 4.2 K used in the experiments. Therefore, the Boltzmann factors (7) are close to unity, the radiative recombination rate is comparable with the spin flip rates, and level anticrossing occurs in fields of $B \lesssim 0.25$ T.

In GaSe crystals and $GaSe_{1-x}Te_x$ solid solutions, the exchange interaction splits the exciton quartet into singlet and triplet by ~ 2 meV with the triplet being additionally split by ~ 0.05 meV in two levels with angular momentum z-components ± 1 (bright exciton) and 0 (dark exciton). One of the bright-exciton levels anticrosses with the dark level in a field of $B \approx 0.5$ T. The radiative and nonradiative recombination times are equal to 1.6 and 10 μs, respectively, and within this time range the exciton spin relaxation can be disregarded [21].

In the GaAs/AlAs heterostuctures studied in this paper and in Ref. [6], the quartet of indirect exciton states is formed by electrons in the conduction X_x-X_y valleys and Γ-point holes. As compared to the previously analyzed nanosystems, the distinctive features of such the excitons are: (i) the radiative exciton times aount to $\sim$ ms, much longer than the spin relaxation times:

$$\tau_{se} = w_e^{-1}, \tau_{sh} = w_h^{-1} \ll \tau_r, \tau_{nr} \, ,$$

(ii) application of magnetic fields can significantly reduce the rates of the electron and hole upward spin flips at low temperatures and make them comparable with the nonradiative decay rate. The level anticrossing in weak magnetic fields is out of the scope of the present work (it takes place at $B < 100$ mT). This particular relation of parameters yields a pronounced interplay of the bright and dark exciton states in the photoluminescence and to the non-trivial circular polarization dependence of the PL on magnetic field and temperature. Below, in Sec. V A, we outline the restrictions on the model parameters needed to successfully reproduce the experimental findings. The theoretical estimate of the heavy-hole g-factor is given in Sec. V B. Further, Sec. VI outlines possible situations which can be realized depending on the relative signs and magnitudes of the electron and hole Landé factors, where one can expect a strong dependence of P_c on magnetic field and temperature.

A. Parameters used for fitting

The exciton recombination in the studied GaAs/AlAs QWs described by Eqs. (12) is governed by eight parameters: the electron (g_e) and heavy hole (g_{hh}) g factors, the recombination times of bright ($\tau_r = 1/w$) and dark ($\tau_{nr} = 1/w'$) excitons, the spin relaxation times for electrons (τ_{se}) and heavy holes (τ_{sh}), the depolarization factor ξ, and the dark-state activation factor C_d. Some of these parameters can be directly measured in experiment, others can be evaluated from fits of various experimental dependencies, or at least the ratio of parameters and their possible ranges of values can be found.

Let us start from well defined parameters. Due to the large band gap at the X point, the spin-orbit contribution to the electron g factor is vanishingly small [16, 22]. As a result, the electron g factor, g_e, is isotropic and its value almost coincides with the free-electron Landé factor of $+2.0$ [23]. The recombination times of the bright and dark excitons were unambiguously determined in Ref. [6], $\tau_r = 0.34$ ms and $\tau_{nr} = 8.5$ ms, by analyzing the PL intensity dynamics and its variation with magnetic field. The solution of Eqs. (12) for pulsed excitation was used to calculate the $P_c(t)$-dynamics with Eq. (11). The analysis of the calculated results demonstrates that the polarization degree rise-time is uniquely determined by the shortest among the electron and hole spin relaxation times and does not depend on other parameters. It will be shown in Sec. VI B, that the sign of P_c in the initial growth stage is unambiguously controlled by the τ_{se}/τ_{sh} ratio. Therefore, the fit of the $P_c(t)$ dynamics presented in Fig. 7(b) allows us to conclude that τ_{se} is longer than $\tau_{sh} = 3 \pm 0.5$ μs, which is valid for all magnetic field strengths and orientations.

Thus, we have four variable parameters to describe the experimental findings: the heavy hole longitudinal g factor g_{hh}, the electron spin relaxation time τ_{se}, and the factors ξ and C_d. However, the possibilities for variation of these parameters are very limited. The factor ξ is unambiguously determined by the saturation level of P_c in tilted magnetic field as shown in Figs. 5 and 6. It equals to 0.75 for the LO_{AlAs} phonon assisted line. The factor C_d together with g_{hh} are responsible for the magnetic field value where the maximum value of the circular polarization degree , $|P_{c,max}|$, is reached in Faraday geometry, see Figs. 2, 3, and 5. An additional restriction is imposed on the heavy hole longitudinal g_{hh} factor. It cannot be smaller than $+2.5$ as recently established from the PL intensity dependence on magnetic field [6]. Finally the electron spin relaxation time τ_{se} defines the slope of the $P_c(B)$ decrease in strong magnetic fields applied in the Faraday geometry as shown in Figs. 2, 3, and 5.

The best fits of $P_c(B)$ and the PL decay at different temperatures, magnetic fields and orientations are shown by the lines in Figs. 2, 3, 4, 5, and 6. All of them are obtained with the following set of parameters: $\tau_{se} = 33 \pm 1$ μs, $C_d = 0.001$, and $g_{hh} = +3.5 \pm 0.1$. In Sec. V B we show that the large positive value of g_{hh} is consistent with a simple estimation based on an effective Hamiltonian approach and with experimental data for short-period GaAs/AlAs superlattices. The parameters used for the model calculations are collected in Table I. It is remarkable that almost perfect quantitative description of all measured experimental dependencies is achieved, which confirms the validity of the used model.

Fitting the experimental data shows that in the studied GaAs/AlAs QW at $T = 1.8$ K the regime of weak magnetic fields is valid for $0 < B < 3$ T and that of moderate magnetic fields for 4 T$< B < 10$ T, see also Fig. 8 and Sec. IV C. One can see in Figs. 3 that the regime

TABLE I. Parameters for the studied ultrathin GaAs/AlAs QWs evaluated either experimentally or from the best fit to the experimental data.

Parameter	Value	Comment
g_e	$+2.0$	[23]
g_{hh}	$+3.5 \pm 0.1$	best fit
τ_r	0.34 ms	[6]
τ_{nr}	8.5 ms	[6]
τ_{sh}	3 ± 0.5 μs	fit in Fig. 7(b)
τ_{se}	33 ± 1 μs	best fit
ξ	0.75	Figs. 5 and 6
C_d	0.001	best fit

of strong magnetic fields, where we can set $\alpha, \beta = 0$, is reached for $B > 12$ T.

Using $C_d = 0.001$ and depolarization factors ξ equal to 0.75 and 0.6, respectively, we obtain excellent fits for all dependencies of the $\mathrm{LO_{AlAs}}$ and $\mathrm{TA_{AlAs}}$ phonon assisted lines. In fact, the $P_c(B)$ dependencies of the LO and TA phonon replicas in Fig. 2 perfectly match each other after scaling by $1/\xi$, which validates the introduction of the replica-dependent depolarization factor in our model. We note that a reasonable description of the no-phonon line is possible for $\xi = 0.31$ and $C_d = 0.001$, but the fit accuracy is significantly smaller for the NP line as compared with the phonon replicas. We exclude this line from consideration because the origin of the NP luminescence is not fully established in our sample [6].

Note that in the fit of the experimental data presented above we assumed that the generation rates in all states are equal $G_{sj_z} \equiv G$. We have checked that accounting for the thermalization of electrons and holes between their spin states in the course of relaxation does not allow us to reproduce the dynamics of polarization and, moreover, in sufficiently strong magnetic fields makes the contribution of the dark states too strong to account for the observed values.

B. Theoretical estimate of the heavy-hole g factor

To calculate the exciton states and their g factor in a monolayer-thick GaAs/AlAs QW one needs an atomistic computation based on a microscopic theory such as a tight-binding model. This is beyond the scope of the present work. Instead, in order to get a crude estimate of the heavy-hole g factor in the ultrathin QW we apply an effective Hamiltonian and take into account the magnetic field-induced mixing of the heavy- and light-hole states. The monolayer-thick QW is modeled by a rectangular heteropotential $V(z)$ with well width $a_0 = 0.565$ nm and GaAs/AlAs valence band offset of $\Delta V = 0.53$ eV [24]: $V(z) = 0$ inside the well and $V(z) = \Delta V$ in the barriers. In such a well there are only one heavy-hole ($hh1$) and one light-hole ($lh1$) quantum-confined subbands. The magnetic-field-induced mixing calculated in the framework of the Luttinger Hamiltonian takes place between subbands of different parity. Therefore, in the evaluation of g_{hh} we have to take into account the linear-in-$\boldsymbol{k}$ mixing of the $hh1$ subband states with the continuum of the light-hole states, where $\boldsymbol{k}$ is the in-plane hole wave vector. Following Ref. [25] (see also Refs. [26, 27]) we represent the g factor of the heavy hole as

$$g_{hh} = -6\tilde{\kappa} + 4\sqrt{3}a_0 \int dz S_h(z) \left\{ \gamma_3 \frac{d}{dz} \right\}_s C_h(z), \quad (29)$$

where $\tilde{\kappa}$ is the average magnetic Luttinger parameter between the two materials, $\{ab\}_s = (ab + ba)/2$ is the symmetrized product of operators, $C_h(z)$ is the envelope wavefunction in the ground $hh1$ subband (with the quantum-confined energy E_{hh1}) and the function $S_h(z)$ describing the $\boldsymbol{k}$-linear light-hole admixture is defined by the equation

$$\left[-\frac{\hbar^2}{2m_0} \frac{d}{dz} (\gamma_1 + 2\gamma_2) \frac{d}{dz} + V(z) - E_{hh1} \right] S_h(z) = - \frac{\sqrt{3}\hbar^2}{m_0 a_0} \left\{ \gamma_3 \frac{d}{dz} \right\}_s C_h(z), \quad (30)$$

with γ_i ($i = 1, 2, 3$) being the Luttinger band parameters. Making use of this shallow quantum-well model we recast g_{hh} in the form

$$g_{hh} = -6\kappa + \frac{\gamma_3^2}{\gamma_1 - 2\gamma_2} \frac{\nu^2}{(1+\nu)^2} \approx 2.67, \quad (31)$$

where $\nu = \sqrt{(\gamma_1 - 2\gamma_2)/(\gamma_1 + 2\gamma_2)}$ and all the Luttinger parameters correspond to those of the AlAs material: $\gamma_1 = 3.76$, $\gamma_2 = 0.82$, $\gamma_3 = 1.42$, and $\kappa = 0.12$ [24]. It is worth stressing, that the final value of g_{hh} differs not only in magnitude but also in sign from the averaged bulk value of -6κ. The positive sign of g_{hh} is determined by the dominant contribution to the g factor arising due to the $\boldsymbol{k}$-linear admixture of continuum light-hole states to the confined heavy-hole states. Thus, g_{hh} is positive and exceeds the value of $g_e \approx 2$ expected for electrons in the X-valleys of AlAs. This result qualitatively agrees with effective Hamiltonian calculations [28] and results of experimental magneto-optical studies of GaAs/AlAs short-period superlattices [29–33]. Particularly, Baranov et al. [30] obtained $g_e = 1.90$, $g_{hh} = 3.2$ in a 0.74 nm/1.43 nm superlattice, and $g_e = 1.88$, $g_{hh} = 3.14$ in a 1.05 nm/2.99 nm sample.

VI. MODEL PREDICTIONS FOR STRUCTURES WITH DIFFERENT SETS OF PARAMETERS

In this section, using the developed model we simulate the experimental appearances in structures with different sets of parameters in order to highlight the variability of possible experimental realizations. This can

serve as a guide for the further search for systems with tailored dependencies of the polarization degree on magnetic field and temperature. We consider scenarios where the electron and hole spin relaxation times are shorter than the recombination time of the bright exciton, to avoid complications related with transient spin relaxation processes. Hereinafter we choose for definiteness the following values of the exciton recombination times: $\tau_r = 0.5$ ms and $\tau_{nr} = 10$ ms in all calculations. For simplicity, we set the depolarization factor $\xi = 1$. As before we neglect the electron-hole exchange interaction.

The PL intensity and exciton dynamics depend strongly on the signs and magnitudes of the electron and heavy-hole g factors [6]. Let us introduce, following the approach used in Ref. 34, the effective g factors of the bright and dark excitons in the Faraday geometry as

$$g_b = g_{hh} - g_e, \quad g_d = g_{hh} + g_e,$$

respectively. g_b describes the splitting of the excitons active in σ^+ and σ^- polarization as $E_{-+} - E_{+-} = g_b \mu_B B_z$, while g_d gives the splitting of the states $++$ and $--$. Provided that $|g_b| > |g_d|$ (*case* 1, illustrated in Fig. 8) the Zeeman splitting of the bright excitons exceeds the splitting of the dark states, so that in a magnetic field $B_z \neq 0$ the lowest state is a bright exciton. By contrast, if $|g_b| < |g_d|$ (*case* 2, Fig. 9), the exciton state lowest in energy is dark.

In the studied GaAs/AlAs QW both g_e and g_{hh} are positive, hence, $g_b < g_d$ and the case 2 is realized. Below we analyze various situations for different relations between the kinetic parameters τ_{se} and τ_{sh}. For illustration of the model predictions we select those dependencies that clearly demonstrate distinct features for the different chosen sets of parameters: the dynamics of the magnetic-field-induced circular polarization degree, the dependence of P_c on temperature and magnetic field orientation at fixed high field strength, and $P_c(B)$ in longitudinal magnetic field and in tilted field geometry with $\theta = 45°$.

A. Case 1, $|g_b| > |g_d|$

For definiteness we assume that $g_e > 0$, $g_{hh} < 0$, and $|g_{hh}| > |g_e|$. The only configuration of the exciton spin levels that is possible in this case in the Faraday geometry is schematically shown in Fig. 9. The dependencies of the selected quantities calculated for the set of parameters given in the figure caption are shown in Fig. 10. When we vary the parameters across wide ranges, namely g_e from 0.1 to 2, g_{hh} from -0.3 to -3, C_d from zero to 0.01, and τ_{se} and τ_{sh} from 0.01 μs to 0.1 ms for fixed values of T and B, all dependencies demonstrate the same trends: (i) after the excitation pulse P_c increases with time up to saturation, with the corresponding time constant being the shorter one of the electron and hole spin relaxation times [Fig. 10(a)]; (ii) P_c monotonically decreases with increasing temperature, in accordance with a Boltzmann

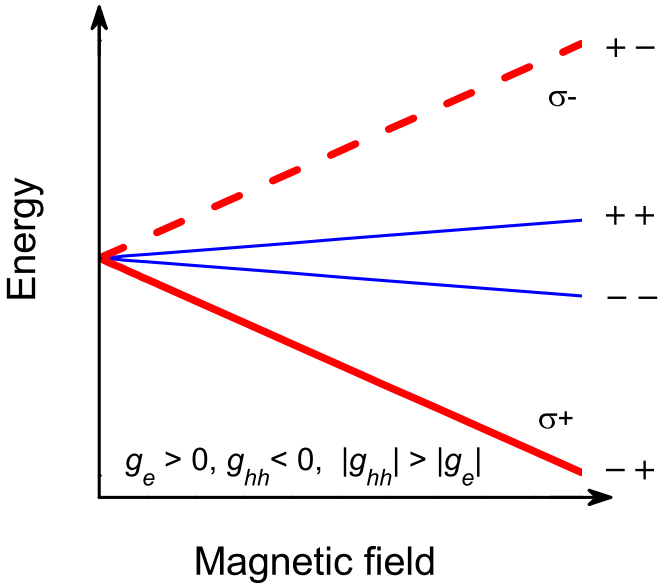

FIG. 9. (Color online) Schematics of the exciton spin levels in the Faraday geometry $\boldsymbol{B} \parallel z$ for the case 1: $g_e > 0$, $g_{hh} < 0$, and $|g_{hh}| > |g_e|$. Blue lines show optically dark (spin-forbidden) states, red lines show spin allowed bright states active in σ^+ (solid line) and σ^- (dash line) polarization.

population of the bright exciton levels [Fig. 10(b)]; (iii) the angular dependence of P_c reflects the Zeeman splitting of the bright exciton levels by projecting the magnetic field on the growth axis of the structure [Figs. 10(c) and 10(d)]. In fact, in this regime the recombination and spin dynamics behaviors of the four-level system reduce to those of a two-level system involving bright states only. The dark states are important as intermediate states only in the course of electron and hole spin relaxation and the reservoir of dark excitons is not formed due to efficient downward spin flip processes towards the optically active exciton state of lowest energy [6], see Fig. 9.

B. Case 2, $|g_b| < |g_d|$

For definiteness we set here $g_e > 0$, $g_{hh} > 0$. The magnetic field applied in the Faraday geometry quenches the PL then, as the dark exciton becomes the lowest energy state. Depending on the system parameters the exciton PL and polarization behaviors become multifaceted. In contrast to the case 1 two possible configurations of exciton spin levels, which differ by the sign of the bright exciton g factor, can be distinguished here, as shown in Fig. 11.

From Sec. IV C, in the range of weak magnetic fields, the P_c behavior is similar to the case of a two-level system and is determined by the Boltzmann population of the bright exciton levels. Therefore, the most interesting scenarios can be found in the ranges of moderate and strong magnetic fields. Since these ranges are determined

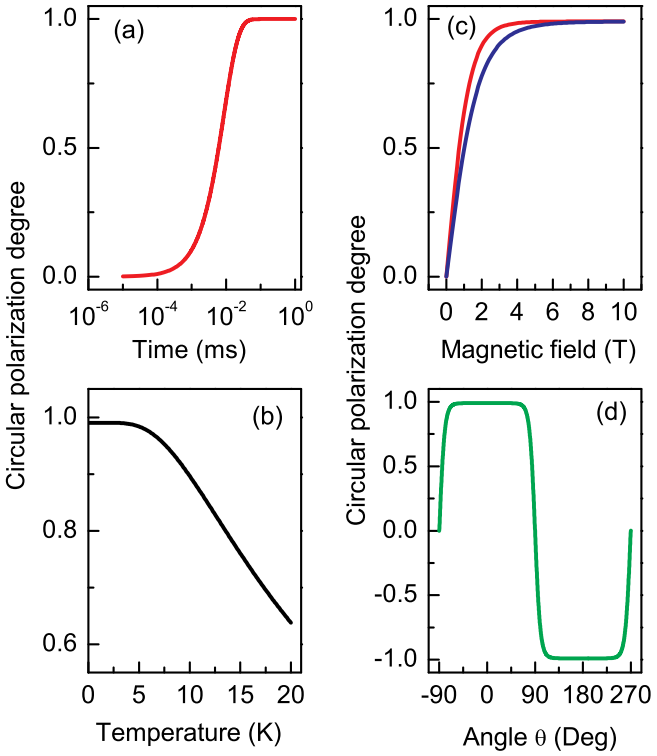

FIG. 10. (Color online) Calculated dependencies for $P_c(B)$: (a) Dynamics of P_c measured in the Faraday geometry. (b) P_c as function of temperature. (c) P_c as function of longitudinal (red line) and tilted by 45° (blue line) magnetic field. (d) P_c as function of tilt angle. Parameters used in the calculations: $T = 2$ K, $B = 10$ T, $g_e = +2$, $g_{hh} = -3$, $C_d = 0.001$, $\tau_{se} = 50$ μs, $\tau_{sh} = 5$ μs, $\tau_r = 0.5$ ms, and $\tau_{nr} = 10$ ms.

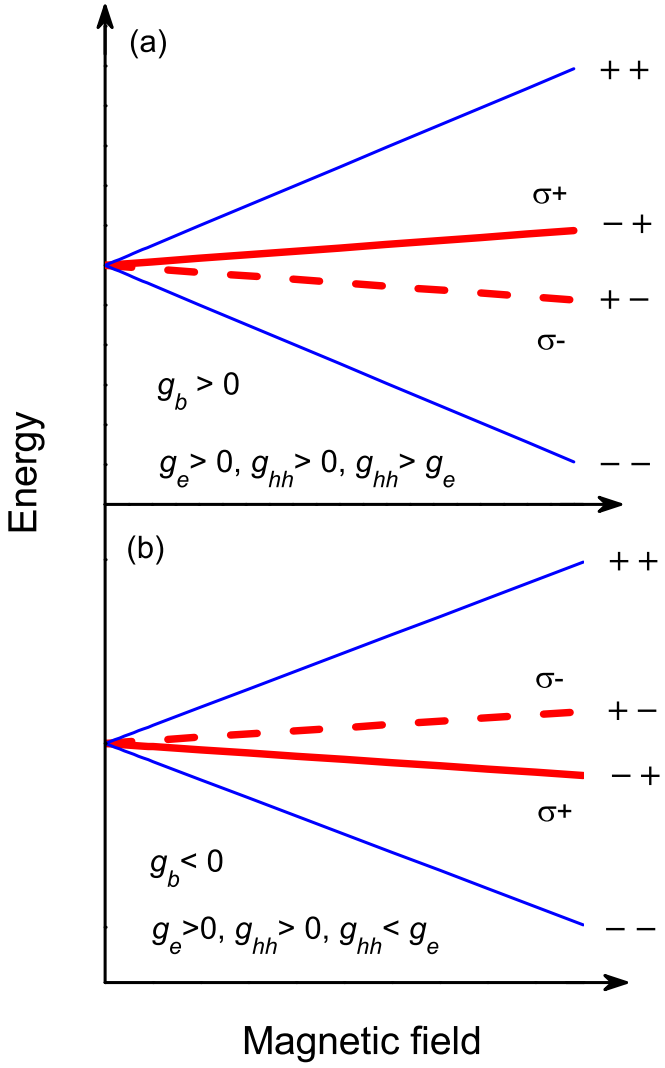

FIG. 11. (Color online) Schematics of exciton spin levels in the Faraday geometry for the case 2: $g_e > 0$, $g_{hh} > 0$, on one case (a) $g_{hh} > g_e$ and in the other case (b) $g_{hh} < g_e$. The blue lines show the optically dark (spin-forbidden) states, the red lines show the spin-allowed bright states active in σ^+ (solid line) and σ^- (dashed line) polarizations.

by the ratio of magnetic ($g\mu_B B_z$) and thermal ($k_B T$) energies we use the following sets of parameters that provide corresponding conditions: $T = 2$ K, $B = 10$ T, $g_e = +2$, $g_{hh} = +2.5$ to provide a positive sign of g_b and $g_{hh} = +1.5$ for a negative sign of g_b. Even the strict selection rules given by Eq. (8) with $C_d = 0$ lead to an interesting behavior of the emission circular polarization degree P_c as function of time t, magnetic field B and temperature T.

Let us start with the $P_c(t)$ dynamics calculated for different ratios of τ_{se}/τ_{sh} shown in Fig. 12. These functions are nonmonotonic. The rise stage is controlled by the shortest spin relaxation time, while the decay stage is determined by the longest one of the electron and hole spin relaxation times. The sign of $P_c(t)$ in the rise stage is determined by the τ_{se}/τ_{sh} ratio and does not depend on the g_b sign. This is because the bright states $+-$ and $-+$ are initially equally populated and their population state dynamics is controlled by the kinetic parameters. Rise-time and decay-time of the polarization degree are correspondingly determined by the shortest and longest among the electron and hole spin relaxation times.

The circular polarization dependence on magnetic field, $P_c(B)$, calculated for the Faraday and for tilted geometries at $T = 2$ K are shown in Fig. 13. Most spectacularly a nonmonotonic behavior with sign reversal is expected for the Faraday geometry, see Figs. 13(a) and 13(b). In weak magnetic fields the slope of $P_c(B)$ and its sign are controlled by g_b. One can see that the dependencies calculated for a varying τ_{se}/τ_{sh} ratio closely follow each other in agreement with Eq. (24). By contrast, in strong magnetic fields the P_c sign and value are again determined by the τ_{se}/τ_{sh} ratio, see Eqs. (22) and (23). Depending on this ratio the $P_c(B)$ dependence can be either monotonic reaching saturation, or nonmonotonic with a sign reversal, but also reaching saturation in strong fields. In the tilted geometry ($\theta = 45°$) the $P_c(B)$ dependences demonstrate only a weak maximum and follow closely each other for the varying values of the τ_{se}/τ_{sh}

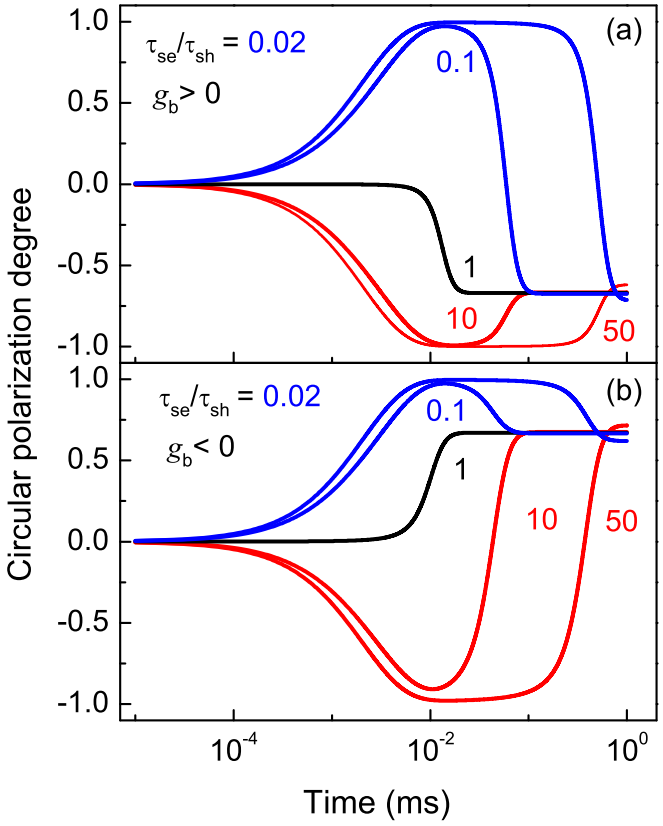

FIG. 12. (Color online) Calculated dynamics of $P_c(t)$ for different ratios of τ_{se}/τ_{sh} with the following fixed parameter set: $T = 2$ K, $B = 10$ T, $C_d = 0$, $\tau_r = 0.5$ ms, $\tau_{nr} = 10$ ms, and $g_e = +2$. (a) $g_{hh} = +2.5$, $g_b > 0$ and (b) $g_{hh} = +1.5$, $g_b < 0$. We use in the calculations $\tau_{se} = 1$ μs for $\tau_{se}/\tau_{sh} \leq 1$ and $\tau_{sh} = 1$ μs for $\tau_{se}/\tau_{sh} \geq 1$.

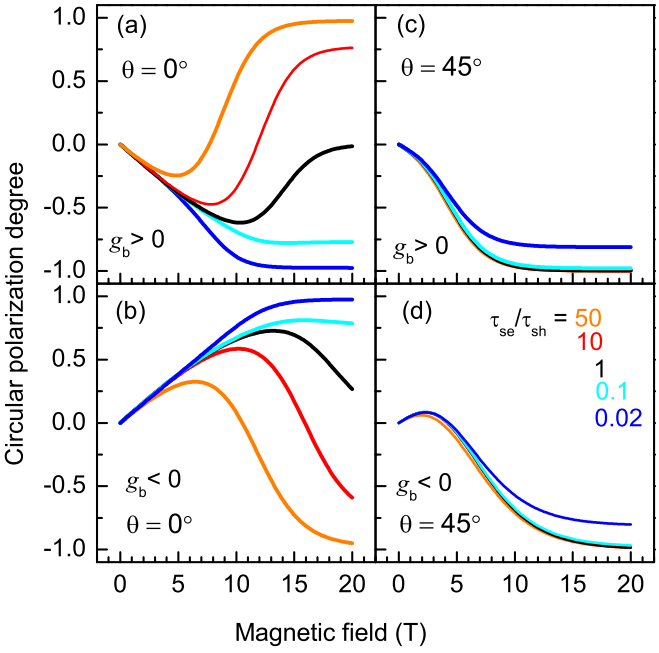

FIG. 13. (Color online) $P_c(B)$ dependencies calculated for different ratios of τ_{se}/τ_{sh} [presented in panel (d)] for $T = 2$ K, $C_d = 0$, $\tau_r = 0.5$ ms, $\tau_{nr} = 10$ ms, and $g_e = +2$. (a) Faraday geometry: $g_{hh} = +2.5$ and $g_b > 0$. (b) Faraday geometry: $g_{hh} = +1.5$ and $g_b < 0$. (c) Tilted geometry: $g_{hh} = +2.5$ and $g_b > 0$. (d) Tilted geometry: $g_{hh} = +1.5$ and $g_b < 0$. We use in the calculations $\tau_{se} = 1$ μs for $\tau_{se}/\tau_{sh} \leq 1$ and $\tau_{sh} = 1$ μs for $\tau_{se}/\tau_{sh} \geq 1$. Note that as before only the Zeeman effect caused by the z component of the magnetic field is taken into account for the heavy holes.

ratio and the sign of g_b, see Figs. 13(c) and 13(d). In fact, as shown in Fig. 14, a significant change of the magnetic field-induced circular polarization degree occurs for the angles θ around the Faraday geometry ($\theta \approx 0°$ and $\theta \approx 180°$), while the mixing of states in tilted geometry neutralizes the contribution of carrier spin-flips on the polarization degree.

The temperature dependencies for P_c in the Faraday geometry are also nonmonotonic and depend strongly on the kinetic parameter τ_{se}/τ_{sh} ratio in the range of strong magnetic fields, see Fig. 15. At high temperatures (above 7 K) where the ratio $g\mu_B B_z/k_B T \ll 1$ we return to the case of Boltzmann population of the bright exciton sublevels, Eq. (24).

C. Case 2. Role of deviation from strict selection rules for optical transitions

Finally, let us have a closer look into the effect expected from a small deviation from the optical selection rules. Here interesting scenarios can arise for moderate and strong magnetic fields when the polarization of the lower dark state emission related with the coefficient C_d in Eq. (28) differs from that of the lower bright state. We assume, similar to the situation revealed for the studied GaAs/AlAs QW, that the state with $m_z = -2$ is weakly active in the σ^+ polarization and, vice versa, the state with $m_z = +2$ is weakly active in the σ^- polarization. The corresponding configuration of the exciton spin levels is shown in Fig. 11(a). The magnetic field dependencies of P_c calculated at T =2 K and for τ_{se}/τ_{sh} =50 using different values of the dark exciton emission activation factor C_d are shown in Fig. 16. The most significant changes occur again for the angles θ close to the Faraday geometry ($\theta \approx 0°$ and $\theta \approx 180°$) at low temperatures, as clearly seen in Fig. 16(b) and 16(d). One can see, that the factor C_d strongly affects the dynamics of $P_c(t)$ in Fig. 16(a) and the $P_c(B)$ dependencies in Fig. 16(c).

The model calculation results presented in Sec.VI demonstrate a great variety of possible experimental dependences of P_c demonstrating that the magnetic-field-induced circular polarization degree is a sensitive tool to decode the spin structure and the spin dynamics of excitons in low dimensional structures.

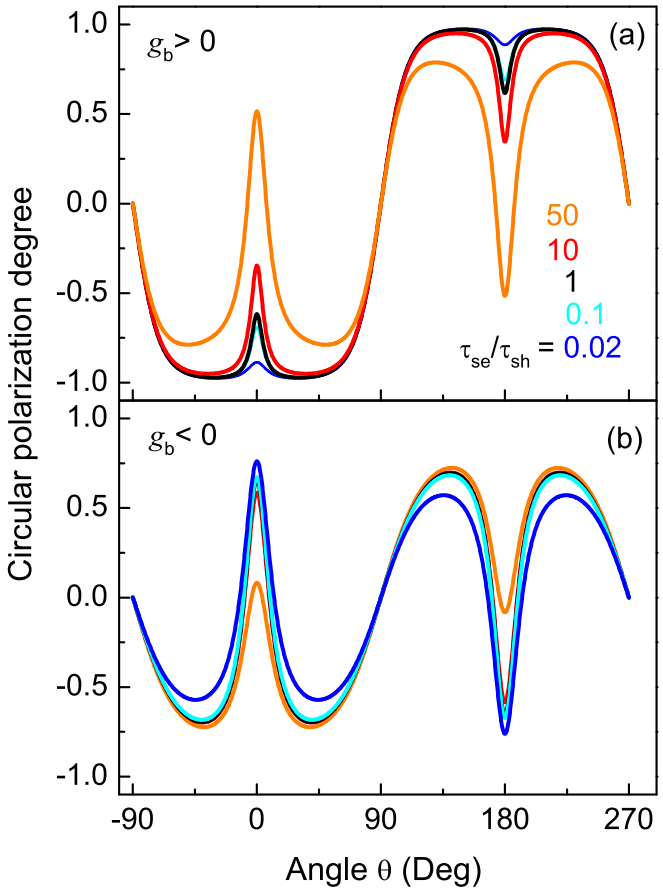

FIG. 14. (Color online) Dependencies of $P_c(\theta)$ calculated for $T = 2$ K and $B = 10$ T, $C_d = 0$, $\tau_r = 0.5$ ms, $\tau_{nr} = 10$ ms, and $g_e = +2$ for different ratios of τ_{se}/τ_{sh} [panel (a)]. (a) $g_{hh} = +2.5$ and a longitudinal value of $g_b > 0$ and (b) $g_{hh} = +2.5$ and a longitudinal value of $g_b < 0$. We use in the calculations $\tau_{se} = 1$ μs for $\tau_{se}/\tau_{sh} \leq 1$ and $\tau_{sh} = 1$ μs for $\tau_{se}/\tau_{sh} \geq 1$. Note that as before only the Zeeman effect caused by the z component of the magnetic field is taken into account for the heavy holes.

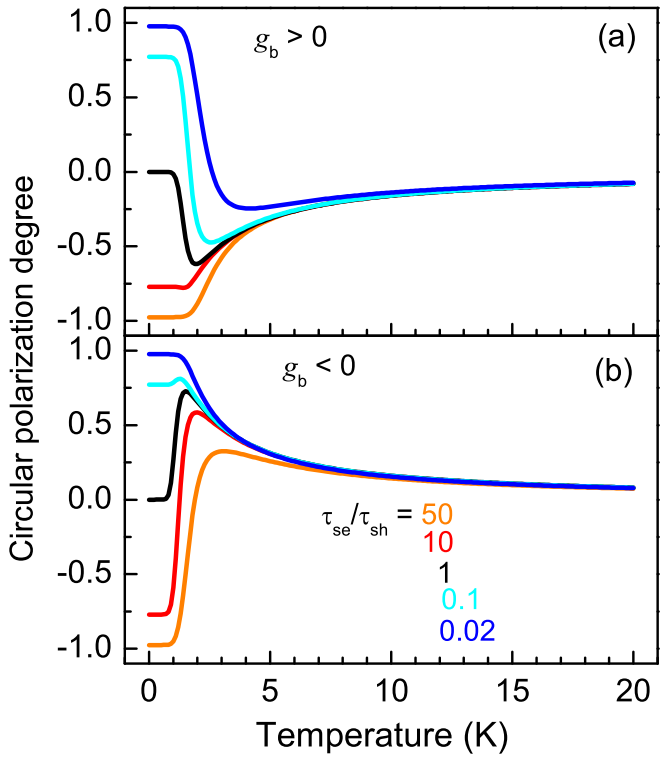

FIG. 15. (Color online) Temperature dependencies of P_c calculated for different ratios of τ_{se}/τ_{sh} (given in panel (b)) in the Faraday geometry at $B = 10$ T, $C_d = 0$, $\tau_r = 0.5$ ms, $\tau_{nr} = 10$ ms, and $g_e = +2$. (a) $g_{hh} = +2.5$, $g_b > 0$ and (b) $g_{hh} = +1.5$, $g_b < 0$. We use in the calculations $\tau_{se} = 1$ μs for $\tau_{se}/\tau_{sh} \leq 1$ and $\tau_{sh} = 1$ μs for $\tau_{se}/\tau_{sh} \geq 1$.

VII. CONCLUSION

We investigated experimentally and theoretically the magneto-optical properties of a two-monolayer-thick GaAs/AlAs quantum well, which is indirect both in real and in $\boldsymbol{k}$ space. The exciton spin dynamics have been addressed through the emission circular polarization induced by external magnetic fields. The extremely long exciton recombination time provided by the spatial separation of electron and hole due to the type-II band alignment in combination with electrons in the X valley results in a novel physical situations. The spin relaxation times of electrons and holes are remarkably long, $\tau_{se} = 33$ μs and $\tau_{sh} = 3$ μs, compared to, e.g., type-I GaAs/(Al,Ga)As QWs. The combination of the system parameters with the nonradiative recombination time being long compared with the radiative one and the possibility to control the rate of transitions from the lower to the upper Zeeman levels by the magnetic fields result in unusual dependences of the emission polarization on the magnetic field and temperature. A kinetic equation model which accounts for the dynamics of the quartet of bright and dark exciton states in the QW with C_{2v} point symmetry provided by the heavy-light hole mixing has been developed. A perfect quantitative description of all experimental data is obtained with just a few variable parameters which can be unambiguously determined from the experimental data. We demonstrate that the magnetic field-induced circular polarization can be controlled either by thermodynamical parameters, i.e., the ratio of the exciton Zeeman splitting and the thermal energy, or by kinetic parameters, i.e., the relations between the various relaxation times in the system, depending on temperature and magnetic field. Furthermore, we have extended the model calculations to varying parameters sets in order to highlight the role of specific parameters in the experimental appearances. The developed approach can readily be used for investigation of the spin dynamics in semiconductor quantum well and quantum dot structures with indirect band gap either in real or in $\boldsymbol{k}$ space, or in both of them.

Acknowledgements We thank M.V. Durnev for valuable discussions. This work was supported by the Ger-

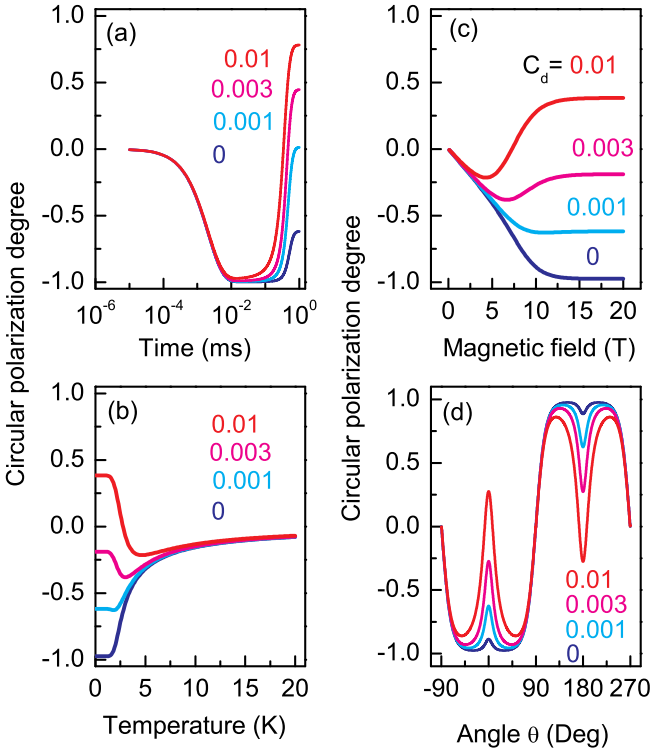

FIG. 16. (Color online) Calculated dependencies of P_c for different factors C_d of the dark exciton emission activation. (a) $P_c(t)$ dynamics in the Faraday geometry. (b) $P_c(T)$. (c) $P_c(B)$ in the Faraday geometry. (d) $P_c(\theta)$. Used parameters in the calculations: $T = 2$ K, $B = 10$ T, $g_e = +2$, $g_{hh} = +2.5$, $\tau_{se} = 50$ μs, $\tau_{sh} = 1$ μs, $\tau_r = 0.5$ ms, and $\tau_{nr} = 10$ ms.

man Ministry of Education and Research (BMBF) (FKZ: 05K13PE1), the Deutsche Forschungsgemeinschaft and the Russian Foundation for Basic Research via ICRC TRR160, the Russian Foundation for Basic Research (Grants No. 16-02-00242, 15-52-12012, and 17-02-00383), the Russian Federation Government Grant No. 14.Z50.31.0021 (leading scientist M. Bayer), and by the Act 211 Government of the Russian Federation (Contract No. 02.A03.21.0006).

[1] *Optics of Semiconductors and Their Nanostructures*, edited by H. Kalt and M. Hetterich (Springer-Verlag, Berlin, 2004).

[2] C. F. Klingshirn, *Semiconductor Optics* (Springer-Verlag, Heidelberg, 2012).

[3] L. P. Fu, F. T. Bacalzo, G. D. Gilliland, R. Chen, K. K. Baja, J. Klem, and D. J. Wolford, Microscopic mechanisms governing exciton-decay kinetics in type-II GaAs/AlAs supperlattices, Phys. Rev. B **52**, 2682 (1995).

[4] A. V. Khaetskii and Yu. V. Nazarov, Spin relaxation in semiconductor quantum dots, Phys. Rev. B **61**, 12639 (2000).

[5] A. V. Khaetskii, and Y. V. Nazarov, Spin-flip transitions between Zeeman sublevels in semiconductor quantum dots, Phys. Rev. B **64**, 125316 (2001).

[6] T. S. Shamirzaev, J. Debus, D. R. Yakovlev, M. M. Glazov, E. L. Ivchenko, and M. Bayer, Dynamics of exciton recombination in strong magnetic fields in ultrathin GaAs/AlAs quantum wells with indirect band gap and type-II band alignment, Phys. Rev. B **94**, 045411 (2016).

[7] We chose for this study a very thin GaAs QW in order to be able to compare its properties to another InAs/AlAs model QW structure, which has an indirect band gap, but a type-I band alignment. Due to strain, high quality InAs/AlAs QWs can be grown with a few monolayer thickness only. This does not represent a crucial limitation for a GaAs/AlAs heterostructure, for which QWs can be grown with wider width.

[8] T. S. Shamirzaev, A. M. Gilinsky, A. K. Kalagin, A. V. Nenashev, and K. S. Zhuravlev, Energy spectrum and structure of thin pseudomorphic InAs quantum wells in an AlAs matrix: Photoluminescence spectra and band-structure calculations, Phys. Rev. B **76**, 155309 (2007).

[9] W. A. J. A. van der Poel, A. L. G. J. Severens, H. W. van Kesteren, and C. T. Foxon, Spin relaxation in type-II GaAs/AlAs quantum wells, Phys. Rev. B **39**, 8552 (1989).

[10] D. Keller, D. R. Yakovlev, B. König, W. Ossau, Th. Gruber, A. Waag, L. W. Molenkamp, and A. V. Scherbakov, Heating of the magnetic ion system in (Zn,Mn)Se/(Zn,Be)Se semimagnetic quantum wells by means of photoexcitation, Phys. Rev. B **65**, 035313 (2002).

[11] *Physics of Group IV Elements and III-V Compounds*, edited by O. Madelung, M. Schulz, and H. Weiss, Landolt-Börnstein Numerical Data and Relationships, New Series, Group III, Vol. 17, pt. a (Springer, Berlin, 1982).

[12] L. M. Woods, T. L. Reinecke, and Y. Lyanda-Geller, Spin relaxation in quantum dots, Phys. Rev. B **66**, 161318 (2002).

[13] Xiayu Linpeng, Todd Karin, M. V. Durnev, Russell Barbour, M. M. Glazov, E. Ya. Sherman, S. P. Watkins, Satoru Seto, and Kai-Mei C. Fu, Longitudinal spin relaxation of donor-bound electrons in direct band-gap semiconductors, Phys. Rev. B **94**, 125401 (2016).

[14] M. Maaref, F. F. Charfi, D. Scalbert, C. Benoit á la Guillaume, and R. Planel, Recombination processes in short-period GaAs-AlAs superlattices of type II, Phys. Stat. Sol. (b) **170**, 637 (1992).

[15] P. Dawson, K. J. Moore, C. T. Foxon, G. W. 't Hooft, and R. P. M. van Hal, Photoluminescence decay time studies of type II GaAs/AlAs quantum well structures, J. Appl. Phys. **65**, 3606 (1989).

[16] E. L. Ivchenko. *Optical spectroscopy of semiconductor nanostructures* (Alpha Science, Harrow UK, 2005).

[17] F. Liu, A. V. Rodina, D. R. Yakovlev, A. Greilich, A. A. Golovatenko, A. S. Susha, A. L. Rogach, Yu. G. Kusrayev, and M. Bayer, Exciton spin dynamics of colloidal CdTe nanocrystals in magnetic fields, Phys. Rev. B **89**, 115306 (2014).

[18] V. V. Belykh, A. Greilich, D. R. Yakovlev, M. Yacob, J. P. Reithmaier, M. Benyoucef, and M. Bayer, Electron and hole g factors in InAs/InAlGaAs self-assembled quantum dots emitting at telecom wavelengths, Phys. Rev. B **92**, 165307 (2015).

[19] R. I. Dzhioev, H. M. Gibbs, E. L. Ivchenko, G. Khitrova, V. L. Korenev, M. N. Tkachuk, and B. P. Zakharchenya, Determination of interface preference by observation of linear-to-circular polarization conversion under optical orientation of excitons in type-II GaAs/AlAs superlattices, Phys. Rev. B **56**, 13405 (1997).

[20] N. G. Romanov, P. G. Baranov, I. V. Mashkov, P. Lavallard, and R. Planel, Optically detected magnetic resonance study of the transition from pseudodirect type-II to type-I GaAs/AlAs superlattices, Solid State Electron. **37**, 911 (1994).

[21] A. N. Starukhin, D. K. Nelson, B. S. Razbirin, D. L. Fedorov, and D. K. Syunyaev, Evolution of the level anticrossing signal in magnetoluminescence of localized excitons in the GaSeGaTe solid solution, Fiz. Tverd. Tela **57**, 1888 (2015) [Phys. Solid State **57**, 1937 (2015)].

[22] I. A. Yugova, A. Greilich, D. R. Yakovlev, A. A. Kiselev, M. Bayer, V. V. Petrov, Yu. K. Dolgikh, D. Reuter, and A. D. Wieck, Universal behavior of the electron g factor in GaAs/Al_xGa_{1-x}As quantum wells, Phys. Rev. B **75**, 245302 (2007).

[23] J. Debus, T. S. Shamirzaev, D. Dunker, V. F. Sapega, E. L. Ivchenko, D. R. Yakovlev, A. I. Toropov, and M. Bayer, Spin-flip Raman scattering of the Γ-X mixed exciton in indirect band gap (In,Al)As/AlAs quantum dots, Phys. Rev. B **90**, 125431 (2014).

[24] I. Vurgaftman, J. R. Meyer, and L. R. Ram-Mohan, Band parameters for III-V compound semiconductors and their alloys, J. Appl. Phys. **89**, 5815 (2001).

[25] M. V. Durnev, Zeeman splitting of light hole in quantum wells: Comparison of theory and experiments, Phys. Solid State **56**, 1416 (2014).

[26] D. M. Hofmann, K. Oettinger, Al. L. Efros, and B. K. Meyer, Magnetic-circular-dichroism study of heavy- and light-hole g factors in $In_xGa_{1-x}As$/InP quantum wells, Phys. Rev. B **55**, 9924 (1997).

[27] M. V. Durnev, M. M. Glazov, and E. L. Ivchenko, Giant Zeeman splitting of light holes in GaAs/AlGaAs quantum wells, Physica E **44**, 797 (2012).

[28] A. A. Kiselev, and L. V. Moiseev, Zeeman splitting of heavy-hole states in III-V and II-VI heterostructures, Phys. Solid State **38**, 866 (1996).

[29] H. W. van Kesteren, E. C. Cosman, W. A. J. A. van der Poel, and C. T. Foxon, Fine structure of excitons in type-II GaAs/AlAs quantum wells, Phys. Rev. B **41**, 5283 (1990).

[30] P. G. Baranov, I. V. Mashkov, N. G. Romanov, P. Lavallard, and R. Planel, Optically detected magnetic resonance of excitons and carriers in pseudodirect GaAs/AlAs superlattices, Solid State Commun. **87**, 649 (1993).

[31] P. G. Baranov, I. V. Mashkov, N. G. Romanov, C. Gourdon, P. Lavallard, and R. Planel, Magnetic resonance and anticrossing of levels of excitons trapped at opposite interfaces in type-II GaAs/AlAs superlattices, JETP Lett. **60**, 429 (1994).

[32] P. G. Baranov, N. G. Romanov, I. V. Mashkov, G. Khitrova, H. M. Gibbs, and O. Lyngnes, Local sensing of GaAs/AlAs superlattices using the optical detection of magnetic resonance and energy level anti-crossing effects, Fiz. Tverd. Tela **37**, 2991 (1995) [Phys. Solid State **37**, 1648 (1995)].

[33] N. G. Romanov and P. G. Baranov, Fine structure of excitons and eh pairs in GaAs/AlAs superlattices at the X–Γ crossover, Nanotechnology **12**, 585 (2001).

[34] G. Bartsch, M. Gerbracht, D. R. Yakovlev, J. H. Blokland, P. C. M. Christianen, E. A. Zhukov, A. B. Dzyubenko, G. Karczewski, T. Wojtowicz, J. Kossut, J. C. Maan, and M. Bayer, Positively versus negatively charged excitons: A high magnetic field study of CdTe/CdMgTe quantum wells, Phys. Rev. B **83**, 235317 (2011).